

## ULTRATHIN PERFECT ABSORBER BASED ON INTEGRATED METAMATERIAL

Tran Tien Lam<sup>1</sup>, Dinh Thi Nga<sup>2</sup>, Dinh Van Thien<sup>3</sup>, Nguyen Sy Khiem<sup>4</sup>,  
Bui Xuan Khuyen<sup>5,6,\*</sup>, Bui Son Tung<sup>5,6</sup>, Vu Dinh Lam<sup>5,6,\*</sup>

<sup>1</sup>Faculty of Physics, Thai Nguyen University of Education, 20 Luong Ngoc Quyen,  
Thai Nguyen city, Viet Nam

<sup>2</sup>Department of Physics and Technology, Thai Nguyen University of Sciences,  
Thai Nguyen city, Viet Nam

<sup>3</sup>Department of Physics, Hanoi University of Mining and Geology, 18 Vien, Ha Noi, Viet Nam

<sup>4</sup>Faculty of Physics, Hanoi University of Science, Ha Noi, Viet Nam

<sup>5</sup>Graduate University of Science and Technology (GUST), 18 Hoang Quoc Viet, Cau Giay,  
Ha Noi, Viet Nam

<sup>6</sup>Institute of Materials Science, VAST, 18 Hoang Quoc Viet, Cau Giay, Ha Noi, Viet Nam

\*Emails: [lamvd@gust-edu.vast.vn](mailto:lamvd@gust-edu.vast.vn), [khuyenbx@ims.vast.ac.vn](mailto:khuyenbx@ims.vast.ac.vn)

Received: 28 May 2020; Accepted for publication: 31 July 2020

**Abstract.** We improved common metamaterial perfect absorber (MPA) by integrating four embedded inductors or replacing four embedded capacitors in the same compact structure. The obtained results confirmed that the lumped-capacitors MPA maintain an extreme thickness  $t = \lambda/940$ , where  $\lambda$  is operating wavelength at 106.3 MHz. Besides, by replacing these capacitors by inductors in the initial designed-MPA structure, we obtained an effective thickness of  $t = \lambda/53$  at 1.9 GHz. Furthermore, we explained the absorption mechanism in terms of the magnetic energy and power loss distributions related to the impedance-matching effect.

**Keywords:** metamaterials, perfect absorption, low frequency.

**Classification numbers:** 2.1.2, 2.2.2, 2.8.2.

### 1. INTRODUCTION

In the past two decades, artificial electromagnetic metamaterials (MMs) have been raised as a highlighted field in advanced-material research, which opens many potential applications and useful solutions for the development of science and technology. Originating from a theoretical model of Veselago in 1968 [1], MMs have shown an advantage beyond natural materials since they can change the basic principles of interaction between material and electromagnetic waves, such as bending the path a light ray by using negative refractive index (NRI) MM, the opposite of the propagation of electromagnetic waves with energy flow or reverse Cherenkov emission [2 - 4]. In particular, after the experiment published by Smith *et al.* in 2000 for the first real NRI MM [5], their potentials were vigorously expanded for many useful applications, for instance,

slow light [6 - 8], super resolutions [9, 10], super lens [11], invisible cloaking [12], storage device [13], wireless power transfers [14], self-driving cars [15] and especial applications based on perfect absorption of electromagnetic waves [16-20].

By the artificial arrangement of electrical and magnetic components (constructed from metal and dielectric materials), the two- or three-dimensional resonance structure (Meta-atoms) might allow the MM to work flexibly through all frequency regions (from the radio to the optical band). In particular, MMs also possess an extremely small unit-cell size compared to their operating wavelength. For example, the first perfect absorption metamaterial (MPA) has a thickness of only  $1/30$  smaller than its operating wavelength ( $\lambda$ ) [16], which is much thinner than the traditional absorbers (where the thickness is limited to  $\lambda/4$ ) [21]. Moreover, the high absorption was achieved as 96 % (at 11.48 GHz) and 88 % (at 11.5 GHz) for simulation and experiment, respectively. These impressive results are attained by the fact that MM allows both effective permeability and effective permittivity to be equal (perfect impedance matching behavior) and to create a strong dispersive medium (large losses), at the same resonant frequency.

In recent years, owing to the explosion of the wireless telecommunication and radio broadcasting, providers and researchers have faced a new challenge in the number of services demanded by their customers, which requires a multi-functionality, reducing the size while maintaining the high-performance in a wide area of devices. There are many effective resolutions of scale-down MM structures with small unit cell, which can be useful for such as improved readability within RFID (radio-frequency identification) portals, 2-D power imaging devices, and wireless power transferring systems [22 - 27]. Unfortunately, in the radio band, most recent MPAs are too thick, large and expensive to be easily integrated in real devices. Based on this dynamic, we proposed an integrated method to realize perfect absorption in the low frequency regions (the radio broadcasting band: 0.1 - 0.4 GHz and the LTE/Bluetooth/WiMAX frequency band: 0.7 – 6.0 GHz).

## 2. MATERIALS AND METHODS

A single unit cell (periodicity of  $A$ ) of our proposed MPA is designed as in Fig. 1(a). The lumped capacitors (or inductors) are integrated at the center of air gaps (width of  $g$ ). The optimized geometrical parameters are selected to be  $A = 30$ ,  $d = 2$ ,  $g = 1.6$  and  $w = 29$  mm. The FR-4 is chosen as a dielectric spacer (thickness of  $t = 3.0$  mm). The optimized meta-surface and continuous-copper layer is shorted by the cylindrical interconnects (at each corner) to attain simultaneously strong resonance and perfect impedance matching at very low frequencies. The simulated results are performed by using the CST Microwave Studio [28], where the absorption can be achieved as  $A = 1 - |T| - |R| = 1 - |S_{21}(\omega)|^2 - |S_{11}(\omega)|^2$ , where  $T = |S_{21}(\omega)|^2$  and  $R = |S_{11}(\omega)|^2$ . Because of continuous metallic layer,  $S_{21}(\omega) = 0$  therefore, the absorption is calculated as  $A = 1 - |R| = 1 - |S_{11}(\omega)|^2$ . In general, the absorption frequency can be adjusted by  $f = 1/[2\pi(LC)^{1/2}]$ , where  $L$  and  $C$  are total effective inductance and capacitance, respectively [29]. Therefore, we carried out two different simulations. The first one is to miniaturize the unit-cell size of absorber by integrating four capacitors. The second one is to scale down the size of absorber (while keeping the same geometrical parameters) by replacing four lumped inductors.

## 3. RESULTS AND DISCUSSION

In the first case (radio broadcasting band), as shown in Fig. 1(b), the lumped capacitor is

changed from 100 to 300 pF. Consequently, high-absorption peaks at 86.9, 95.2, 106.3, 122.7 and 150.2 MHz at the normal incidence are obtained corresponding to absorption of 93.7, 98.4, 99.4, 98.8 and 93.5 %, respectively. In other words, the periodicity is significantly miniaturized

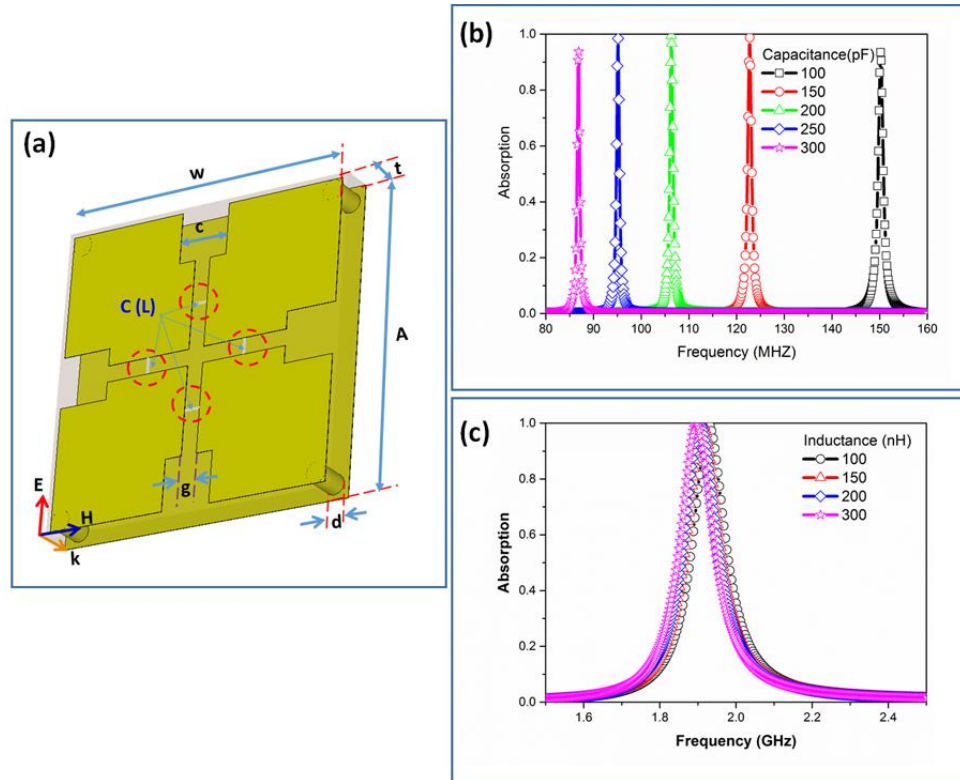


Figure 1. (a) Schematic of the single unit cell of proposed MPA. Simulated absorption spectra in sync with the variation of (b) lumped capacitors and (c) lumped inductors.

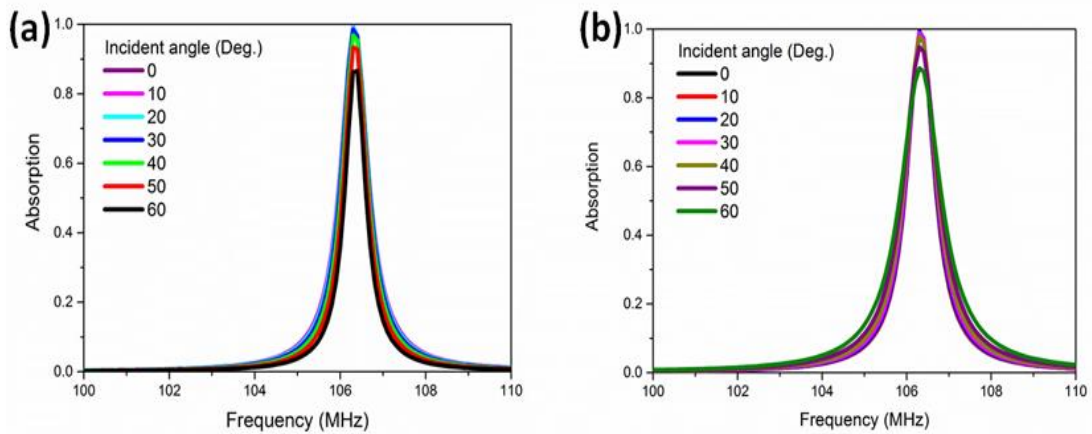


Figure 2. Simulated absorption spectra according to the incident angle of EM wave in case of (a) the TE and (b) the TM polarization, for  $C = 200$  pF.

to be  $A = \lambda/115, \lambda/105, \lambda/94, \lambda/81.4$  and  $\lambda/66.5$ , respectively, with respect to these absorption frequencies. Particularly, the absorber is miniaturized to be  $t = \lambda/1150, \lambda/1050, \lambda/940, \lambda/814$  and

$\lambda/665$  for thickness, respectively. In the second case (LTE/Bluetooth/WiMAX region), as presented in Fig. 1(c), the simulated result yields an absorption over 99.6 % at 1.89, 1.90, 1.91 and 1.93 GHz since lumped inductance is changed from 100 to 300 nH. The ratios of thickness and lattice constant of MPA to the longest wavelength are reduced to be  $t = \lambda/53$  and  $A = \lambda/5.3$ , respectively. Therefore, it can be noted that, in order to maintain the high absorption while reducing the unit-cell size of MPA, the value of lumped capacitance (or inductance) should be higher in the specific range.

For the optimized capacitance,  $C = 200$  pF, the influence of oblique angle ( $\Theta$ ) of incidence on absorption is estimated as showed in Fig. 2. The absorption of 99.4 % (at 106.3 MHz) when  $\Theta = 0$  reduces to 86 % and 88.6 % at  $\Theta = 60^\circ$  for the transverse-electric (TE) and the transverse-magnetic (TM) polarizations, respectively. These behaviors confirmed that the proposed MPA conserves well the high absorption in a wide range of incident angles. In case of  $L = 200$  nH, a 90%- absorption peak is maintained at an incident angle up to  $40^\circ$  for the TE polarization and  $50^\circ$  for the TM polarization, as shown in Fig. 3. Interestingly, since  $\Theta$  is changed from  $30$  to  $60^\circ$  (TM polarization), a new absorption peak (absorption over 87%) is raised at lower frequency as presented in Fig. 3(b). To facilitate the comparison between lower-frequency absorption peak and higher-frequency one, they can be regarded as a contribution of two separated resonators (the left- and the right-half of MPA, along the external electric field) in case of large incident angle of EM wave. The near-field coupling between these resonators leads to the distribution of induced magnetic energy density not to be uniform. In case of the strongest near-field coupling, for example at  $\theta=30^\circ$ , we observed the distribution of magnetic density similarly to the magnetic resonance of whole structure, at 1.79 GHz. In the other case, the distribution of induced magnetic energy density is similar to the magnetic resonances of the left- and the right-half of structure, at 1.9 GHz (not shown here). Since the incident angle of electromagnetic wave is larger (from  $40$  to  $60^\circ$ ), the left (or the right) resonator plays dominant role for the dual-band absorption corresponding to the direction of incident angle with respect to the normal direction of sample plane. Consequently, the magnitude and the peak-position of absorption spectra are slightly changed. These behaviors confirm that the proposed MPA can be flexibly operated in different frequency bands by only changing lumped components.

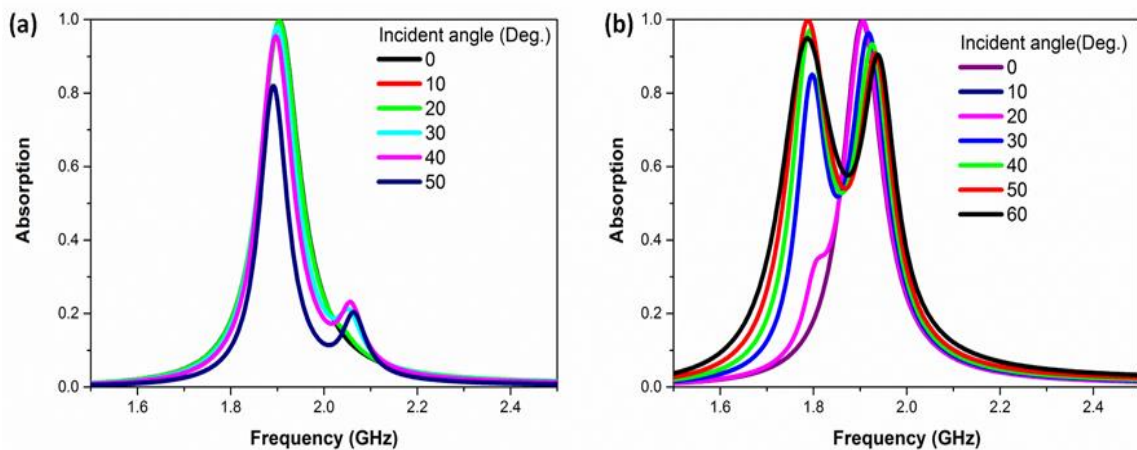


Figure 3. Evolution of absorption spectra according to the incident angle of EM wave in case of (a) the TE and (b) the TM polarization, for  $L = 200$  nH.

The underlying mechanism of proposed MPA is visualized by the magnetic-energy and power-loss-density distributions at 106.3 MHz [Figs. 4(a) and 4(b)] and at 1.9 GHz [Figs. 4(c) and 4(d)]. The 3-dimensional views in Figs. 4(a) and 4(c) show a strong magnetic resonance is formed as expected in the shorted MPA by the interconnection of the cylindrical copper wires at each corner. In other words, a nearly-perfect absorption for both cases is caused from the magnetic resonances raised at frequencies of the perfect impedance matching. It can be remarked that the dielectric loss plays a dominant role for consuming the energy of incoming EM wave. As simulated in Figs. 4(b) and 4(d), along the excited electric-field ( $\mathbf{E}$ ) direction, the magnitude of induced power loss, which is proportional to the induced surface current, is ordinarily enhanced nearby the left-right capacitor (or inductor) areas.

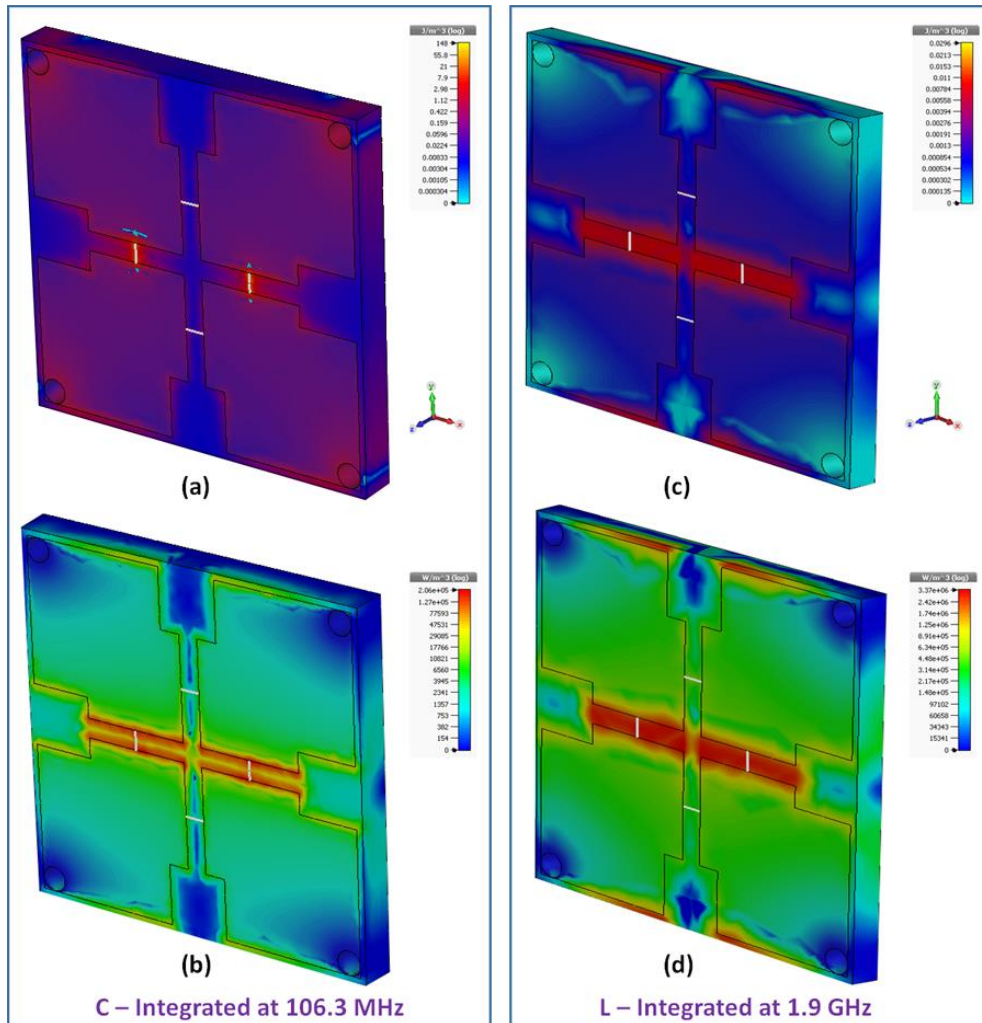


Figure 4. 3-dimensional distributions for the induced magnetic energy and the power loss at (a)-(b) 106.3 MHz and (c)-(d) 1.9 GHz.

#### 4. CONCLUSIONS

A common MPA is efficiently miniaturized to have ultra-small unit-cell size (periodicity of  $0.01\lambda$  and thickness of  $0.001\lambda$  at 103.6 MHz). The stable performance of proposed MPA

(absorption over 90%) is tested for all the TE and TM polarizations by the of incident angle of EM radiation up to 60°. Particularly, by switching the lumped elements built-in initial structure, we flexibly tuned the absorption feature in different frequency ranges. Both types of integrated MPAs confirm that two absorption peaks (absorption about 90%) can be well maintained for an incident angle below 50°. Thus, we believed that the proposed MPAs, introduced in this study, can be widely utilized in order to realize the meta-devices for the future radio/telecommunication applications.

**Acknowledgements.** This research is funded by Vietnam National Foundation for Science and Technology Development (NAFOSTED) under grant number 103.99-2018.332 and by Institute of Materials Science, Vietnam Academy of Science and Technology under grant number HTCBT.05/20-20.

## REFERENCES

1. Veselago V. G. - The electrodynamics of substances with simultaneously negative values of  $\epsilon$  and  $\mu$ , *Sov. Phys. Usp.* **10** (1968) 509.
2. Ziolkowski R. W. - Pulsed and CW Gaussian beam interactions with double negative metamaterial slabs, *Opt. Express* **11** (2003) 662.
3. Chen J., Wang Y., Jia B., Geng T., Li X., Feng L., Qian W., Liang B., Zhang X., and Gu M. - Observation of the inverse Doppler effect in negative-index materials at optical frequencies, *Nature Photonics* **5** (2011) 239.
4. Duan Z. Y., Wu B.-I., Xi S., Chen H., and Chen M. - Research progress in reversed cherenkov radiation in double-negative metamaterial, *PIER* **90** (2009) 75.
5. Smith D., Padilla W. J., Vier D., Nemat-Nasser S. C., and Schultz S. - Composite medium with simultaneously negative permeability and permittivity, *Phys. Rev. Lett.* **84** (2000) 4184.
6. Thuy V. T. T., Tung N. T., Park J. W., Lam V. D., Lee Y. P., and Rhee J. Y. - Highly dispersive transparency in coupled metamaterials, *J. Opt.* **12** (2010) 115102.
7. Jang M. S. and Atwater H. - Plasmonic rainbow trapping structures for light localization and spectrum splitting, *Phys. Rev. Lett.* **107** (2011) 207401.
8. Wu C., Khanikaev A. B., and Shvets G. - Broadband slow light metamaterial based on a double-continuum fano resonance, *Phys. Rev. Lett.* **106** (2011) 107403.
9. Fang N., Lee H., Sun C., and Zhang X. - Sub-diffraction-limited optical imaging with a silver superlens, *Science* **308** (2005) 534.
10. Scarborough C. P., Jiang Z. H., Werner D. H., Rivero-Baleine C., and Drake C. - Experimental demonstration of an isotropic metamaterial super lens with negative unity permeability at 8.5 MHz, *Appl. Phys. Lett.* **101** (2012) 014101.
11. Pendry J. B. - Negative refraction makes a perfect lens, *Phys. Rev. Lett.* **85** (2000) 3966.
12. Schurig D., Mock J. J., Justice B. J., Cummer S. A., Pendry J. B., Starr A. F., and Smith D. R. - Metamaterial electromagnetic cloak at microwave frequencies, *Science* **314** (2006) 977.
13. Driscoll T., Kim H. T., Chae B. G., Kim B. J., Lee Y. W., Jokerst N. M., Palit S., Smith D. R., Ventra M. D., and Basov D. N. - Memory metamaterials, *Science* **325** (2009) 1518.

14. Lee W. S., Lee H. L., Oh K. S., and Yu J. W. - Uniform magnetic field distribution of a spatially structured resonant coil for wireless power transfer, *Appl. Phys. Lett.* **100** (2012) 214105.
15. Fitzek F., Rasshofer R. H., Biebl E. M. - In: *Proceedings of 2010 European Microwave Conference (EuMC)*, London: Horizon House Publications Ltd., (2010) 1401–1404.
16. Landy N. I., Sajuyigbe S., Mock J. J., Smith D. R., and Padilla W. J. - Perfect metamaterial absorber, *Phys. Rev. Lett.* **100** (2008) 207402.
17. Hoa N. T. Q., Tuan T. S., Hieu L. T., and Giang B. L. - Facile design of an ultra-thin broadband metamaterial absorber for C-band applications, *Sci. Rep.* **9** (2019) 468.
18. Kalraiya S., Chaudhary R. K., and Abdalla M. A. - Design and analysis of polarization independent conformal wideband metamaterial absorber using resistor loaded sector shaped resonators, *J. Appl. Phys.* **125** (2019) 134904.
19. Khuyen B.X., Tung B.S., Tung N.T., Hien N.T., Kim Y.J., Chen L.Y., Lee Y.P., Linh P.T., Lam V.D. - Realization for dual-band high-order perfect absorption, based on metamaterial. *J. Phys. D: Appl. Phys.* **53** (2020) 105502.
20. Khuyen B. X., Tung B. S., Kim Y. J., Hwang J. S., Kim K. W., Rhee J. Y., Lam V. D., Kim Y. H., and Lee Y. P. - Ultra-subwavelength thickness for dual/triple-band metamaterial absorber at very low frequency, *Sci. Rep.* **8** (2018) 11632.
21. Munk B. A., *Frequency Selective Surfaces: Theory and Design* (Wiley-Interscience, New York, 2000).
22. Okano Y., Ogino S., and Ishikawa K. - Development of optically transparent ultrathin microwave absorber for ultrahigh-frequency RF identification system, *IEEE Trans. Microwave Theory Tech.* **60** (2012) 2456.
23. Yagitani S., Katsuda K., Nojima M., Yoshimura Y., and Sugiura H. - Imaging radio-frequency power distributions by an EBG absorber, *IEICE Trans. Commun.* **E94-B** (2011) 2306.
24. Costa F., Genovesi S., and Monorchio A. - A chipless RFID based on multiresonant high-impedance surfaces, *IEEE Trans. Microwave Theory Tech.* **61** (2013) 146.
25. Costa F., Genovesi S., Monorchio A., and Manara G. - Low-cost metamaterial absorbers for sub-GHz wireless systems, *IEEE Antennas Wireless Propag. Lett.* **13** (2014) 27.
26. Yoo Y. J., Zheng H. Y., Kim Y. J., Rhee J. Y., Kang J.-H., Kim K. W., Cheong H., Kim Y. H., and Lee Y. P. - Flexible and elastic metamaterial absorber for low frequency, based on small-size unit cell, *Appl. Phys. Lett.* **105** (2014) 041902.
27. Zuo W., Yang Y., He X., Zhan D., and Zhang Q. - A miniaturized metamaterial absorber for ultrahigh-frequency RFID system, *IEEE Antennas Wireless Propag. Lett.* **PP(99)** (2016) 1.
28. CST of America, Inc., 492 Old Connecticut Path, Suite 505, Framingham, MA 01701, USA. <http://www.cst.com>
29. Zhou J., Economou E. N., Koschny T., and Soukoulis C. M. - Unifying approach to left-handed material design, *Opt. Lett.* **31** (2006) 3620.